Journal of Hydrology 549 (2017) 50–61

Contents lists available at ScienceDirect

Journal of Hydrology

journal homepage: www.elsevier.com/locate/jhydrol

Research papers

Hydrogeochemistry and geothermometry of deep thermal water in the carbonate formation in the main urban area of Chongqing, China

Pingheng Yang [a,b,*], Qun Cheng [c], Shiyou Xie [a,b], Jianli Wang [a,b], Longran Chang [d,*], Qin Yu [a,b], Zhaojun Zhan [a,b], Feng Chen [a,b]

[a] School of Geographical Sciences, Southwest University, Chongqing Key Laboratory of Karst Environment, Key Laboratory of Eco-environments in Three Gorges Reservoir, Ministry of Education of the People's Republic of China, Chongqing 400715, China
[b] Field Scientific Observation and Research Base of Karst Eco-environments at Nanchuan in Chongqing, Ministry of Land and Resources of China, Chongqing 408435, China
[c] Nanjiang Hydrogeological Team under the Chongqing Bureau of Geology and Minerals Exploration, Chongqing 401120, China
[d] College of Resources and Environment, Southwest University, Chongqing 400715, China

ARTICLE INFO

Article history:
Received 2 August 2016
Received in revised form 21 January 2017
Accepted 24 March 2017
Available online 30 March 2017
This manuscript was handled by L. Charlet, Editor-in-Chief, with the assistance of Nico Goldscheider, Associate Editor

Keywords:
Thermal water
Carbonate rocks
Water-rock interaction
Geothermometry
Regional groundwater flow
Chongqing
China

ABSTRACT

Many geothermal reservoirs in Chongqing in southwestern China are located in carbonate rock aquifers and exploited through drilling. Water samples from 36 geothermal wells have been collected in the main urban area of Chongqing. Chemical types of the thermal water samples are Ca·Mg-SO_4 and Ca-SO_4. High contents of Ca^{2+} and SO_4^{2-} in the thermal water samples are derived from the dissolution of evaporates. Furthermore, the HCO_3^- concentration is constrained by the common ion effect. Drilling depth has no effect on the physical and chemical characteristics according to the results of a *t*-test. The geothermal reservoir's temperature can be estimated to be 64.8–93.4 °C (average 82 °C) using quartz and improved SiO_2 geothermometers. Values of δD and $\delta^{18}O$ for the thermal water samples indicate that the thermal water resources originate from local precipitation with a recharge elevation between 838 and 1130 m and an annual air temperature between 10.4 and 13.9 °C. A conceptual model of regional scale groundwater flow for the thermal water is proposed. The thermal water mainly originates from the meteoric water recharged in the elevated areas of northeastern Tongluoshan and Huayingshan by means of percolation through exposed carbonate before becoming groundwater. The groundwater is heated at depth and moves southwest along the fault and the anticlinal core in a gravity-driven regime. The thermal water is exposed in the form of artesian hot springs in river cutting and low-elevation areas or in wells.

© 2017 Elsevier B.V. All rights reserved.

1. Introduction

Geothermal energy is a type of clean energy that consists of heat, minerals, and water. It is characterized by its wide distribution, low levels of pollutants, direct utility, renewability, and significant environmental and economic effects. The global development of geothermal energy has become especially rapid since the 1970s (Lund et al., 2011). In response to the serious issues of population expansion, energy shortages, and environmental pollution, the exploration and exploitation of geothermal energy have attracted an increasing amount of attentions.

There are numerous geothermal reservoirs in China with vast potential for exploitation and utilization. The potential geothermal resources in the major sedimentary basins in China are approximately 2.5×10^{22} J, and the amount of exploitable geothermal energy is approximately 7.5×10^{21} J (Kong et al., 2014; Wang et al., 2015). The annual exploitable hydrothermal resources are estimated to be 1.8×10^{19} J, which is equivalent to a reduction of 1.4×10^{8} t CO_2 emission (Kong et al., 2014; Wang et al., 2015); of this quantity, the hot spring releases a total of 6.6×10^{17} J annually, which is equivalent to 2.26×10^{7} t of standard coal or a reduction of 5.93×10^{7} t CO_2 emissions (Wang et al., 2015). Until 2014, China had found approximately 4000 hot water points (including hot springs, drilling, and mine water resources) with water temperatures above 25 °C (Zhao and Wan, 2014).

Chongqing municipality was named "the hot springs capital of China" in April 2011, due to its plentiful thermal water resources (Cheng et al., 2015). The area containing thermal water is approximately 1×10^{4} km^2 (Cheng et al., 2015). The thermal water is

* Corresponding authors at: No. 2 Tiansheng Road, Beibei District, Chongqing 400715, China.
E-mail addresses: pinghengyang@126.com (P. Yang), 156791585@qq.com (Q. Cheng), xiesy@swu.edu.cn (S. Xie), wangjl@swu.edu.cn (J. Wang), 544288987@qq.com (L. Chang), 869753197@qq.com (Q. Yu), 1499246985@qq.com (Z. Zhan), 1829484437@qq.com (F. Chen).

http://dx.doi.org/10.1016/j.jhydrol.2017.03.054
0022-1694/© 2017 Elsevier B.V. All rights reserved.

thought to form by means of non-volcanic heating and can emit 3.32×10^{11} kcal/yr (1.9×10^{12} kJ/yr), which is equivalent to 4.75×10^{4} t/yr of standard coal (Wang et al., 2015). The exploitation of the thermal water resources in Chongqing has focused on carbonate strata in the main urban area. The Bei hot spring has been used since the Song dynasty, and the Nan hot spring was exploited in the Ming dynasty. The Dong hot spring, later called the Xi hot spring, has become increasingly famous. Now, there are 107 areas with thermal water resources in Chongqing, including 65 geothermal wells, 26 hot springs, and 16 geothermal mining waters (Li and Liu, 2011). In 2012, the Chongqing Municipal Government planned to develop 10 groups of springs in five locations in the main urban area and 100 hot springs and thermal wells within a one-hour drive from the city center. However, from the mid-1980s to the early 1990s, the discharge and temperature of the water in the hot springs decreased rapidly due to overexploitation. Some of the springs even dried up. Despite this interest, little has been published on the thermal water resources in Chongqing, China, except the work of Li and Liu (2011), Xiao et al. (2015), and Cheng et al. (2015) in Chinese. However, these studies focus only on individual cases (Xiao et al., 2015) and on the general chemical characteristics and quantity of thermal water resources on a regional scale (Li and Liu, 2011; Cheng et al., 2015; Xiao et al., 2015).

The widely applicable fundamental tools for studying thermal water include regional scale hydraulics, water chemistry, ^{2}H and ^{18}O isotopic composition, and geothermometry. Studies on regional scale groundwater hydraulics can be traced back to Tóth (1962, 1963), and the subject has been further developed by a series of researchers (e.g., Zijl, 1999; Jiang et al., 2011). The relationship between groundwater temperature distribution and a single flow system in a unit basin was first studied by Domenico and Palciauskas (1973). According to Tóth (1995), a subsurface rock body can be considered to be hydraulically continuous on a given time scale. The concept of hydraulic continuity can help us to interpret carbonate reservoirs as a whole without separate warm and cold fluids and confined and unconfined parts. Evaluating the regional scale groundwater hydraulics and hydraulic continuity could be useful in geothermal exploration (Mádl-Szőnyi and Tóth, 2015; Mádl-Szőnyi and Simon, 2016). Typically, different flow systems differ greatly in hydrochemistry and isotopes (Tóth, 2009). Therefore, the interaction and mixing of thermal water and surface water can be determined using the concentrations of major ions and the values of $\delta^{18}O$ and δD to trace the origin of the thermal water (e.g., Lee et al., 2011; Wang et al., 2013; Pérez-Zárate et al., 2015; Chatterjee et al., 2016). The geothermometers currently used to efficiently estimate reservoir temperatures include cation geothermometers, e.g., K-Mg (Giggenbach, 1988), Na-K (Can, 2002), Na-K-Ca (Fournier and Truesdell, 1973), and Na-Li thermometers (Fouillac and Michard, 1981); silica (quartz and chalcedony) geothermometers (Fournier, 1977); isotope geothermometers (Millot and Négrel, 2007); and gas geothermometers (D'Amore et al., 1993).

In this study, we focus on characterizing the geochemistry of thermal water in 36 wells in the carbonate rock aquifer in the main urban area of Chongqing, identifying the sources of the major ions to estimate the reservoir temperature based on different geothermometric methods, and setting up a conceptual regional model for the circulation of thermal water. In addition, deep carbonate rock aquifers, most of which are to some degree karstified, are probably the most important thermal water resources outside of volcanic areas (Goldscheider et al., 2010). The deep karst aquifers in China containing hot water are ideal targets for future exploitation and utilization due to their favorable characteristics, which include a high single-well yield, low salinity, easy reinjection, and fewer environmental effects when exploited (Kong et al., 2014). Therefore, studying the thermal water resources in carbonate strata in the main urban area of Chongqing can also provide useful references for the national strategy of geothermal energy exploitation in carbonate formations.

2. Study area description

The Chongqing municipality is situated at the transitional area between the Tibetan Plateau and the middle and lower plains of the Yangtze River basin (Fig. 1a). The main urban area of Chongqing is located in the western part of the Chongqing municipality; they consist of nine districts, including Yuzhong, Jiangbei, Yubei, Banan, and Beibei, etc. The total area is 5473 km^2, and the population is 8.348 million in 2015. Our study area is in the southwestern valley between parallel mountains in the eastern Sichuan basin, i.e., in the eastern Sichuan fold belts with an alternative anticline and syncline distribution (Fig. 1). Within this area, the anticlines form mountains and the synclines form valleys. In general, the pattern is characterized as "one mountain with two valleys and three ridges" or "one mountain with one valley and two ridges." Geomorphologically, the altitude gradually decreases from the northwest to the southwest in the study area. Ridges in the northwest are 700–1300 m a.s.l., whereas the ridges in the southwest vary between 500 and 600 m a.s.l. The Yangtze River, functioning as the local base level of erosion, runs through the study area from southwest to northeast. The Jialing River (one tributary of the Yangtze River) discharges into the Yangtze River at the center of the study area.

From west to east, there are five anticlines in the main urban area: the Wentangxia anticline, the Guanyinxia anticline, the Tongluoxia anticline, the Nanwenquan anticline, and the Taozidang anticline (Fig. 1b). The Wentangxia anticline is long and linear with an "S"-shaped axis. The axis of the Guanyinxia anticline spreads from north-northeast to southwest with strata that are inclined gently in the east and steeply in the west. The southern end of the Tongluoxia anticline is connected to the Nanwenquan anticline by a slanted saddle that exhibits a typical box-shaped structure with an axis oriented 10–20° northeast; and this formation is steep in the east and gentle in the west. The axis of the Nanwenquan anticline has an arc-shaped distribution and is oriented north-northeast to south-southwest; it is gentle in the east wing and steep in the west wing. The axis of the Taozidang anticline is arc-shaped and slightly raised in the west. Geothermal resources are plentiful along these anticlines, and thermal water resources are distributed along both edges of them (Fig. 1b).

The geothermal system in the study area consists of geothermal reservoir, geothermal cap (the cover), and bottom layer. The geothermal reservoir is the aquifer for energy storage and heat transport. In this area, the geothermal reservoir is comprised of sections II (T_1j^2), III (T_1j^3), and IV (T_1j^4) of the Lower Triassic Jianglingjiang Formation, the Middle Triassic Leikoupo Formation (T_2l), and section I (T_1j^1) of the Lower Triassic Jianglingjiang Formation; its total thickness is 540 m. The petrologic composition of T_1j is limestone, dolomite, and gypsum-salt breccia, whereas the petrologic composition of T_2l is dolomitic limestone and aqueous mica clay stone with an emerald color at the bottom. The hydraulic conductivity of the karst aquifer was calculated as 2.2×10^{-5} m/s based on a pumping test conducted in 2014. Both groups of dissolvable carbonates show well-developed karst conduits and corrosion fissures, which imply a good geothermal reservoir.

The geothermal cap (cover) consists of Upper Triassic Xujiahe Formation (T_3xj) clastic rock, a coal layer (the first cover, with a thickness of 375–425 m), and Jurassic (J) red sand and mudstone strata (the second cover, with a thickness of >1000 m). T_3xj and

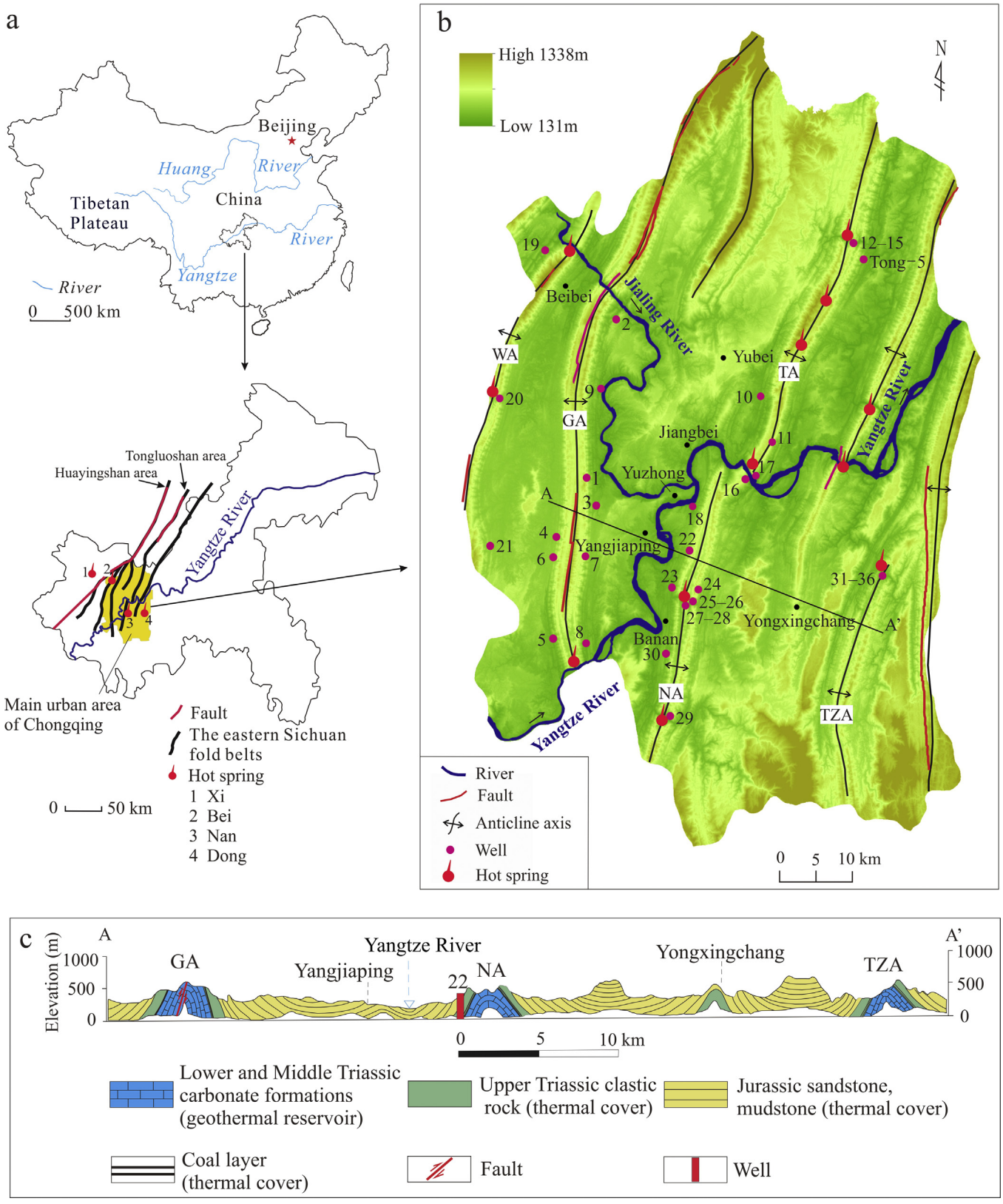

Fig. 1. (a) Location and main structural pattern of the main urban area of Chongqing. The outcrops in the Tongluoshan and Huayingshan areas are the suggested recharge zone for the thermal water of the study area. (b) General geology and DEM of the study area with sampling locations (after Cheng et al., 2015). The sample numbers are shown in Table 1. Numbers 12–15, 25–26, 27–28, and 31–26 are very close together. (c) Geologic section of A-A′ showing an alternative anticline and syncline distribution. The anticlines and synclines mainly consist of carbonate and clastic rock, respectively. WA: Wentangxia anticline, GA: Guanyinxia anticline, TA: Tongluoxia anticline, NA: Nanwenquan anticline, TZA: Taozidang anticline.

the Jurassic strata are located above $T_1j + T_2l$ and are characterized by poor thermal and water conductivity that, to some extent, prevents thermal loss in the geothermal reservoir and forms a layer with low permeability.

The bottom of the geothermal reservoir consists of lower Triassic Feixianguan Formation (T_1f) carbonate and clastic sediment. The petrology is mud limestone and shale with a thickness over 500 m. The shale layer exhibits poor porosity, low permeability, and low thermal conductivity.

The 36 geothermal wells in this study are distributed within the 2 km surrounding the axis of the Wentangxia, Guanyinxia, Tongluoxia, Nanwenquan, and Taozidang anticlines (Fig. 1b).

The study area features a subtropical wet monsoon climate with an average temperature of 17 °C. The annual precipitation is heavy and peaks during late spring and summer; its annual average ranges from 1000 to 1400 mm (Bai et al., 2014).

3. Methods

3.1. Sample collection and experimental analysis

Water samples from the 36 thermal wells (Fig. 1b) were collected by pumping during the wet season in 2009. Each sample's temperature, pH, and total dissolved solids (TDS) were measured in the field with uncertainties of 0.1 °C, 0.1 unit, and 1 mg/L, respectively. The concentrations of Ca^{2+}, Mg^{2+}, and SO_4^{2-} were measured using the EDTA titration method with relative errors of ±1%, ±1%, and ±0.6%, respectively. The concentrations of K, Na, and Li were determined using flame atomic absorption spectrophotometry with an accuracy of 0.1 mg/L. The Cl^- concentration was analyzed using argentometric titration with a relative error of ±1%. The SiO_2 concentration was tested using Si-Mo yellow spectrophotometry with a relative standard deviation of 0.5%. The HCO_3^- concentration was determined by titration with a relative error of ±1.6%. All the elemental concentrations were measured at the Geotechnical Engineering Testing Center of Chongqing in accordance with the *Determination Method for Underground Water* published by the Chinese government (The Geological and Mineral of the People's Republic of China, 1993).

No. 2 was collected during the dry season on December 17, 2009, and the other 35 samples were collected during the wet season in 2009. The values of $\delta^{18}O$ and δD of nos. 2, 4, 15, 16, 26, 32 and 33 were obtained using a DELTA V Plus isotope ratio mass spectrometer connected with a GasBench II (Thermo Fisher Scientific Inc., Bremen, Germany). Both international and laboratory isotopic standards were utilized with external uncertainties of less than 0.2‰. The isotopic ratios were reported in delta (δ) notation relative to the V-SMOW standard and expressed in per mil (‰). These measurements were made at the Laboratory of Geochemistry and Isotopes, Southwest University, Chongqing, China.

3.2. Data processing

3.2.1. Saturation index (SI)

The SI was calculated using Phreeqc version 3 (Parkhurst and Appelo, 2013). When SI < 0, the solution is considered undersaturated. When SI = 0, the solution is saturated, and equilibrium is achieved between mineral dissolution and precipitation. When SI > 0, the solution is oversaturated, and extra minerals precipitate.

3.2.2. t-test for independent samples and correlation analysis

The *t*-test for independent samples is designed to compare two independent samples from normal populations to test whether the mean and variance of the samples' sources are the same (e.g., Schipper and McGill, 2008). When Sig > 0.05, the difference between the samples is insignificant; when Sig < 0.05, the difference between the samples cannot be ignored.

Correlation coefficient analysis is used to measure the strength of the association between two continuous variables. A Pearson rank correlation analysis (two-tailed) was used to examine the possible correlations among various physical and chemical parameters.

The *t*-test and the correlation coefficient analysis were performed using IBM SPSS statistics 19.0.

3.2.3. Geothermometry

The geothermometric calculations of the reservoir temperatures used in this study are as follows:

Quartz (Fournier, 1977): $T_{SiO2} = [1309/(5.19 - \lg S)] - 273.15$,
Chalcedony (Fournier, 1977): $T_{SiO2} = [1032/(4.69 - \lg S)] - 273.15$,
Improved SiO_2 (Verma and Santoyo, 1997): $T_{SiO2} = -44.119 + 0.24469S - 1.7414 \times 10^{-4}S^2 + 79.305\lg S$,
K-Mg (Giggenbach, 1988): $T_{K\text{-}Mg} = 4410/[14 - \lg(K^2/Mg)] - 273.15$,
Na-Li (Fouillac and Michard, 1981): $T_{Na\text{-}Li} = 1049/[\lg(Na/Li) + 0.44] - 273.15$,
Na-K (Giggenbach, 1988): $T_{Na\text{-}K} = 1390/[1.75 - \lg(Na/K)] - 273.15$, and
Na-K-Ca (Fournier and Truesdell, 1973): $T_{Na\text{-}K\text{-}Ca} = 1647/\{\lg(Na/K) + (4/3)[\lg(\sqrt{}Ca/Na) + 2.06] + 2.47\} - 273.15$,

where S is the concentration of SiO_2 in the water (mg/L), and K, Mg, Na, Li, and Ca represent the concentrations (mg/L) of the corresponding elements.

3.2.4. Circulation depth

$$Z = (T_Z - T_0)/G + Z_0, \quad (1)$$

where Z is the circulation depth (m); T_z is the temperature of the geothermal reservoir calculated by a reasonable geothermometer (°C); T_0 is the local annual average temperature (°C); G is thermal gradient (°C/m); and Z_0 is the thickness of the constant temperature zone (m). The average temperature in this area is 17 °C, as mentioned above, and therefore, T_0 = 17 °C, Z_0 = 0, and G = 0.03 °C/m (Cheng et al., 2015) here.

3.2.5. Recharge altitude and its annual average air temperature based on δD

Because the study area has a regional scale, the recharge altitude and its annual average air temperature can be calculated using the general equation for China (Zhou et al., 2010):

$$\delta D = -0.03ALT - 27, \quad (2)$$

$$\delta D = 3T - 92, \quad (3)$$

where ALT is the altitude (m), and T is the annual air temperature (°C) in the recharge area.

4. Results

4.1. Hydrogeochemistry of the thermal water samples

The physical and chemical indexes of the 36 thermal water samples in the study area are presented in Table 1. Except for no. 21 (−7.32%), the relative uncertainties of all the ion equilibria are less than 5% (Table 1). The cation molarity ($TZ^- = HCO_3^- + 2\text{-}SO_4^{2-} + Cl^-$) is 24.3–47.6 meq/L, and the anion molarity

Table 1
Physical and chemical parameters of the thermal water samples. The water temperature (T) is in °C; the TDS and major element concentrations are in mg/L; the well depth is in m; the error in the anion and cation imbalance (E) is in %; and the cation and anion molarities are in meq/L; – denotes species that were not analyzed.

Sample ID no.	T	pH	TDS	K^+	Na^+	Ca^{2+}	Mg^{2+}	HCO_3^-	Cl^-	SO_4^{2-}	SiO_2	Li	Cation molarity	Anion molarity	E	Well depth
1	32.5	7.5	1895	9.9	6.3	329.4	145.1	233.3	4.1	1220	20.6	0.205	28.9	28.8	0.17	700
2	40	7.7	2833	17.5	8.1	651.9	120	157.1	4.1	1903	24.6	0.178	43.3	41.5	2.05	1300
3	57	7.3	2775	17.7	20.5	614.8	109.7	183.5	11.2	1844	31.8	0.25	41.1	40.9	0.2	1718
4	52	7.4	2720	28.3	30.4	633.9	100.3	164.8	5.3	1779	29.2	0.346	42.0	39.2	3.49	2160
5	48	7.6	2715	23.4	13.9	641.9	80.4	195.9	4.1	1793	29.3	0.404	39.9	39.9	0	1778
6	51	7.6	2904	22.3	25.2	663.1	115.8	168.3	6.8	1910	30.8	0.355	44.3	41.9	2.8	2080
7	50	7.7	2875	22.3	46.6	604.7	109.4	160.2	9.6	1945	26.1	0.413	41.8	42.6	−0.9	1866
8	55	7.4	2508	23.2	36.8	549	85.2	174.2	8.2	1653	32.6	0.324	36.7	36.8	−0.21	2336
9	52	7.5	2665	18.7	13.4	600.5	118.4	166.4	2.3	1761	32.1	0.184	40.8	38.7	2.64	1910
10	52	7.6	1710	8.8	27.8	358.3	71.6	219.5	19.6	1043	27.9	0.156	25.2	25.4	−0.38	2178
11	24.5	8.1	375	2.4	1.6	77.5	29.2	342.1	2.7	31.5	40.7	0.053	6.4	6.3	0.63	1139
12	48	7.7	2458	21.9	52.9	535.8	90.1	186.6	24	1577	34.4	0.224	37.1	35.9	1.58	349
13	53	8.2	2530	23.2	47.6	547.6	81.4	169.1	26	1634	36.2	0.212	36.8	36.9	−0.15	118
14	48	7.6	1930	15.6	36.2	408.5	72	236.4	17.5	1213	26.2	0.164	28.3	29.1	−1.39	200
15	49	7.8	2345	22.9	52.1	488	104.2	206	27.6	1483	33.8	0.23	35.8	34.4	2.01	486
16	41	7.4	3035	12.5	55.4	623.8	166.6	171.1	45.1	1982	34.4	0.231	47.6	44.5	3.37	518
17	41	7.3	2686	11.7	44.9	585.6	122.9	195.9	43.7	1711	26.2	0.19	41.6	39.4	2.81	227
18	38	8.4	3030	12.9	52.3	641.9	128.6	162.7	46.4	1983	35.2	0.206	45.3	44.5	0.93	701
19	35	7.7	2097	4.9	11.4	457.9	92	213.2	11.9	1372	21.9	0.11	31.1	31.8	−1.16	1570
20	37	7.5	1620	4.4	6.3	379.3	60.5	223.6	2.7	1005	22.9	0.082	24.3	24.3	0.15	556
21	41	7	387	15.9	3.1	82.5	4.1	150.4	42.7	104.1	27.5	<0.1	5.0	5.8	−7.32	2053
22	52	7.7	2660	12.9	39.3	575.6	131.5	170.4	26.6	1731	26.2	0.17	41.6	38.9	3.45	1981
23	57	7.6	2650	16.1	44.7	594.1	90.1	194.4	24.6	1716	34	0.179	39.5	38.9	0.72	1918
24	50	7.7	2758	23.1	170.1	509.2	114.5	159.2	109	1676	40.7	0.362	42.9	39.9	3.59	2156
25	45	7.6	2158	10.2	35.9	465.7	101.6	195.9	24.6	1340	34.4	0.154	33.5	31.3	3.43	519
26	42	8.1	2240	10.1	38.4	485.6	94	187.5	28.7	1430	28	0.112	33.9	33.1	1.3	55
27	44	7.9	2350	10.8	17.9	531.5	111.3	219.6	10.9	1485	40.7	0.132	36.8	34.2	3.63	329
28	45	7.7	2362	10.4	17.4	541.1	108.1	212.7	10.9	1514	26.2	0.138	37.0	34.7	3.17	417
29	40	7.7	2816	9.7	35.1	697.6	59.5	186.6	21.9	1840	31	0.15	41.5	41.2	0.38	71
30	42	7.6	2780	10.4	34.6	599.4	119	188.2	24.6	1840	31.1	0.154	41.5	41.3	0.24	188
31	51.5	7.7	2820	15.3	21.6	632.3	123.5	171.1	9.6	1877	40.1	0.244	43.1	41.4	2.06	384
32	54.5	7.7	3008	15.9	22.5	625.9	130.6	168	10.4	2048	40.7	0.24	43.4	44.8	−1.6	173
33	52	7.9	2936	15.2	22.7	668.4	86.8	171.1	9.6	1977	39.8	0.234	41.9	43.4	−1.73	126
34	52	7.5	2840	15	23.9	647.2	113.9	168	9	1874	41.2	0.251	43.2	41.3	2.25	375
35	52	7.4	2795	15.3	22.8	640.8	110	168	8.2	1844	39.5	0.233	42.5	40.6	2.25	332
36	50	8.1	2910	15.1	24.3	645.8	109.6	166	10.9	1938	41.2	0.212	42.8	42.6	0.21	316

($TZ^+ = Na^+ + K^+ + 2Ca^{2+} + 2Mg^{2+}$) is 24.3–45.6 meq/L, with the exception of nos. 11 and 21. The cation and anion molarities are exceptionally low compared to the rest of the thermal water samples, with values of 6.4 meq/L and 6.3 meq/L, respectively, for no. 11, and values of 5 meq/L and 5.8 meq/L, respectively, for no. 21. Except for nos. 11 and 21, the major cations are Ca^{2+} and Mg^{2+}, which occur at concentrations of 329.4–697.6 mg/L and 59.5–166.6 mg/L, respectively, and with their proportions of 62.3–84.5% and 7.4–29.6%, respectively. The main anion is SO_4^{2-}, which occurs at a concentration of 1005–2048 mg/L and in a proportion of 81.4–92.2%. The concentration of HCO_3^- is as low as 157–236 mg/L, and its proportion is 7.4–18.2%. Except for Nos. 11 and 21, the TDSs of the thermal water samples are between 1620 and 3035 mg/L. The thermal water samples are generally brackish and contain significantly higher concentrations of SO_4^{2-} and Ca^{2+} than the shallow karst water (fresh water) in Chongqing (Yang et al., 2013).

Piper plots of the major cations and anions (Fig. 2) were used to map the hydrogeochemical facies of the thermal water samples. All the samples are of the Ca·Mg-SO_4 or Ca-SO_4 type, except Nos. 11 and 21 which contain Ca·Mg-HCO_3 and Ca-HCO_3·SO_4. The TDS and ion molarity in nos.11 and 21 are much lower than the values from other wells (Table 1), which is explained by the great impact of the mixture of shallow karst water characterized by Ca-HCO_3^- or Ca·Mg-HCO_3^-.

As shown in Table 1, except for no. 11, the thermal water samples have medium-low temperatures in the range from 32.5 to 57.0 °C. The pH range from 7.3 to 8.4 indicates weak alkalinity.

The depths of the drill wells range from 55.4 to 2336 m (Table 1). To check whether the physical and chemical properties

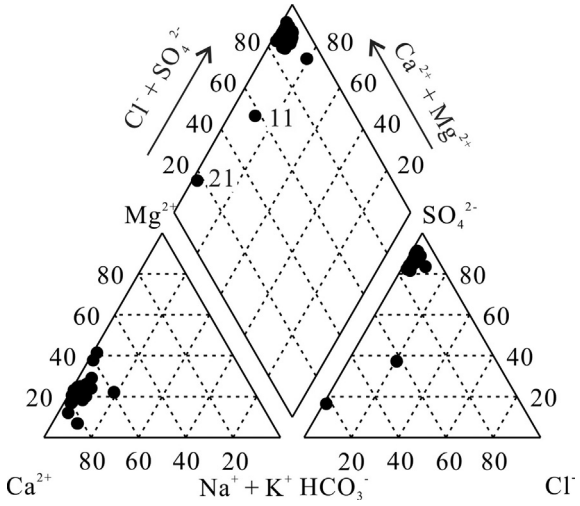

Fig. 2. Piper plot of the thermal water samples. All the samples are of the Ca·Mg-SO_4 or Ca-SO_4 type, except nos. 11 and 21, whose chemical types are Ca·Mg-HCO_3 and Ca-HCO_3·SO_4, respectively.

of these 36 thermal water resources are influenced by depth, we arbitrarily classified each well as deep (depth ≥ 1000 m) or shallow (depth < 1000 m). The independent sample *t*-test was performed on the physical and chemical data collected from the deep wells and the shallow wells. As shown by the results in Table 2, the confidence is always >0.05, which implies that there

Table 2
Independent sample *t*-test of the physical and chemical parameters of shallow (depth < 1000 m) and deep (depth ≥ 1000 m) wells. The water temperature (T) is in °C; and the TDS and major ion concentrations are in mg/L.

Parameter	Deep well	Shallow well	*t*	Sig.
T	42.9	47.8	−1.33	0.19
pH	7.73	7.57	1.71	0.1
K^+	13.3	17.2	−1.98	0.06
Na^+	31	32.9	−0.2	0.85
Ca^{2+}	561.7	507.7	1.08	0.29
Mg^{2+}	106.8	91.5	1.46	0.15
HCO_3^-	189.1	188	0.09	0.93
Cl^-	19.4	19.3	0.02	0.98
SO_4^{2-}	1667	1484	1.15	0.26
TDS	2560	2309	1.16	0.25
SiO_2	33.5	30.4	1.51	0.14
Li	0.19	0.23	−1.25	0.23

are no significant differences in the physical and chemical properties of deep and shallow wells. Therefore, the drilling depth has no effect on the properties of the thermal water samples, which demonstrates that all the thermal water comes from a hydrogeological system characterized by the regional hydraulic continuity that is more effective in the carbonate basin due to the higher hydraulic diffusivity of the carbonates (Mádl-Szőnyi and Tóth, 2015).

Table 3 shows the results of the correlation analysis of the physical and chemical parameters. The small correlation coefficients between the depth and each index imply that depth has an insignificant effect on the physical and chemical properties of the thermal water resources, which is consistent with the results inferred from the independent sample *t*-test. The TDS is highly correlated with the concentrations of SO_4^{2-}, Ca^{2+}, and Mg^{2+}; the correlation coefficients are 0.99, 0.98, and 0.86, respectively. The correlation coefficients of the SO_4^{2-} concentration with the concentrations of Ca^{2+} and Mg^{2+} are 0.98 and 0.74, respectively. Negative correlations were observed for the concentration of HCO_3^- with the concentrations of SO_4^{2-}, Ca^{2+}, and Mg^{2+}; their correlation coefficients are −0.65, −0.63, and −0.37, respectively. Moreover, the high coefficient of 0.87 between the concentrations of Cl^- and Na^+ is indicative of strong correlation.

4.2. Geothermometry

The temperature ensures the geothermal utilization of water in the reservoirs. Table 4 shows the temperature of the thermal water samples calculated using different geothermometers. The temperatures determined using quartz (Fournier, 1977) are 64.6–93 °C. The chalcedony geothermometer (Fournier, 1977) provides temperatures of 32.6–62.4 °C. The improved SiO_2 geothermometer (Verma and Santoyo, 1997) yields temperatures of 65.1–93.7 °C. The temperatures derived from cation geothermometers, including K-Mg (Giggenbach, 1988), Na-Li (Fouillac and Michard, 1981), Na-K (Giggenbach, 1988), and Na-K-Ca (Fournier and Truesdell, 1973) geothermometers, are 28–89.5 °C, 64–271.8 °C, 291.9–1301.7 °C, and 111.7–394.3 °C, respectively.

4.3. Saturation index

Table 5 presents the results of the thermodynamic equilibrium SI. The SIs of anhydrite, gypsum, halite, pyrite, and siderite are less than 0; they imply unsaturation. The oversaturation of secondary minerals, such as goethite, hematite, and talc, can be observed. The SI of chalcedony is in the range from −0.1 to 0.4, which indicates that the solution varies between oversaturation and undersaturation, whereas the SIs for calcite, dolomite, and quartz are >0; they imply oversaturation. Quartz is oversaturated but close to saturation (Table 5). In the correlation between the SiO_2 and temperature graph (Fig. 3), the data points of thermal water fall between the solubility curves of quartz and amorphous SiO_2, which demonstrates that quartz is oversaturated at surface and shallow temperatures, and saturated at still higher temperatures at depth (Majumdar et al., 2009). The data points of the thermal water are aligned neither horizontally to reflect conductive cooling nor along the inclination to reflect cooling dilution (Fig. 3; Majumdar et al., 2009; Chatterjee et al., 2016). These results probably imply that the conductive cooling and diluted cooling of the thermal water are coupled in the upflowing thermal water.

4.4. ^2H and ^{18}O isotopic composition

Table 6 shows the values of δD and $\delta^{18}O$ in seven typical thermal water samples: δD is in the range from −50.3 to −60.9‰ with an average of −56.3‰, and $\delta^{18}O$ is in the range from −7.6 to −9.2‰ with an average of −8.4‰. These fairly stable values of isotopic composition are indicative of a similar hydrogeological genesis for the thermal water, which further supports the results of the *t*-test.

5. Interpretation and discussion

5.1. Origin of the major ions in thermal water

Thermal water can be considered a kind of evolved water whose initial composition has been changed by physical-chemical

Table 3
Correlation analysis of the physical and chemical indexes of the thermal water samples. T is the water temperature.

	T	pH	K^+	Na^+	Ca^{2+}	Mg^{2+}	HCO_3^-	Cl^-	SO_4^{2-}	TDS	SiO_2	Li	Depth
T	1	−0.35*	0.46**	0.2	0.28	0.1	−0.32	0.04	0.28	0.28	0.02	0.37*	0.28
pH		1	−0.15	0.11	0.13	0.05	0.17	0.01	0.13	0.14	0.35*	−0.06	−0.37*
K^+			1	0.35*	0.44**	0.14	−0.62**	0.1	0.45**	0.45**	0.16	0.77**	0.39*
Na^+				1	0.2	0.24	−0.3	0.87**	0.27	0.33	0.27	0.4*	0.12
Ca^{2+}					1	0.63**	−0.63**	−0.07	0.98**	0.98**	0.23	0.60**	−0.16
Mg^{2+}						1	−0.37*	0.09	0.74**	0.74**	0.08	0.43*	−0.16
HCO_3^-							1	−0.26	−0.65**	−0.64	−0.1	−0.44**	−0.13
Cl^-								1	0	0.06	0.16	0.04	0.08
SO_4^{2-}									1	0.99**	0.22	0.65**	−0.15
TDS										1	0.24	0.65**	−0.15
SiO_2											1	0.17	−0.27
Li												1	0.32
Depth													1

* Correlation is significant at the 0.05 level (2-tailed).
** Correlation is significant at the 0.01 level (2-tailed).

Table 4
Temperatures of the thermal water samples determined using different geothermometers. The reservoir temperature is the average calculated using quartz and improved SiO_2 geothermometers. The circulation depth is in m; all other values are in °C; –: no datum.

Sample ID no.	SiO_2 geothermometers			Cation geothermometers				Reservoir temperature	Circulation depth
	Quartz (Fournier, 1977)	Chalcedony (Fournier, 1977)	Improved SiO_2 (Verma and Santoyo, 1997)	K-Mg (Giggenbach, 1988)	Na-Li (Fouillac and Michard, 1981)	Na-K (Giggenbach, 1988)	Na-K-Ca (Fournier and Truesdell, 1973)		
1	64.6	32.57	65.1	39.1	271.8	440.3	163.1	64.8	1579.1
2	71.4	39.69	72.1	52.5	226.3	394.2	130.4	71.8	1806.8
3	81.8	50.56	82.6	53.6	172.5	551.4	150	82.2	2151.6
4	78.3	46.89	79.1	64.8	167	535.2	177.1	78.7	2036.1
5	78.4	46.97	79.2	63.1	257.6	430	153.1	78.8	2039.4
6	80.5	49.19	81.3	58	184.8	545.6	157.2	80.9	2108.7
7	73.8	42.17	74.5	58.6	147.7	698.8	177	74.2	1886
8	82.8	51.67	83.6	62.2	147.2	623.8	185.5	83.2	2184.6
9	82.3	51.09	83.1	54	182.3	461.2	148.1	82.7	2168.1
10	76.5	44.95	77.2	43.6	116.7	840.7	173.8	76.8	1975.1
11	92.5	61.92	93.2	28	271	449.5	222.7	92.9	2503.1
12	85.2	54.17	86	60.3	99.7	744.2	191.7	85.6	2263.8
13	87.3	56.43	88.1	62.8	102.6	693.3	190.6	87.7	2333.1
14	74	42.34	74.7	55.4	103.7	730.5	196.2	74.3	1892.6
15	84.4	53.28	85.2	59.7	102.1	725.4	204.8	84.8	2237.4
16	85.2	54.17	86	42.3	98.8	987.2	147.8	85.6	2263.8
17	74	42.34	74.7	44.1	99.7	917.3	147.6	74.3	1892.6
18	86.2	55.21	87	45.5	95.6	943.9	145.8	86.6	2296.8
19	67	35.02	67.5	30.3	154.1	731.7	111.7	67.2	1658.3
20	68.6	36.7	69.2	32.2	178.3	596.6	114.7	68.9	1712.7
21	75.8	44.26	76.6	89.5	–	291.9	394.3	76.2	1953.6
22	74	42.34	74.7	45.4	101	823.6	151.7	74.3	1892.6
23	84.6	53.55	85.4	53.8	96.5	790.6	161.4	85	2244
24	92.5	61.92	93.2	58.9	63.9	1301.7	224.9	92.9	2503.1
25	85.2	54.17	86	43.2	100.5	882.5	159.1	85.6	2263.8
26	76.6	45.08	77.4	43.8	79.4	914	155.8	77	1980
27	92.5	61.92	93.2	43.4	134.6	635.5	138.6	92.9	2503.1
28	74	42.34	74.7	43.1	139.8	636.1	135.1	74.3	1892.6
29	80.8	49.49	81.6	47.5	100.3	893.9	120.3	81.2	2118.6
30	80.9	49.61	81.7	42	102.6	860.6	135.8	81.3	2121.9
31	91.8	61.17	92.6	49.3	166.5	595.8	141.3	92.2	2481.6
32	92.5	61.92	93.2	49.6	161.7	596.5	144.7	92.9	2503.1
33	91.5	60.85	92.2	52.9	159.1	608.8	136.9	91.9	2470.1
34	93	62.44	93.7	49.8	160.5	625.7	139.9	93.4	2519.6
35	91.2	60.52	91.9	50.6	158.3	609.2	141	91.6	2460.2
36	93	62.43	93.7	50.3	146.5	628.1	140.7	93.3	2519.6

processes (Goldscheider et al., 2010). High concentration of SO_4^{2-} frequently occurs in thermal water discharged from carbonate aquifers (Gunn et al., 2006; Goldscheider et al., 2010). As shown in Table 1 and Fig. 2, SO_4^{2-} and Ca^{2+} are the dominant anion and cation, respectively, in the thermal water samples, and the concentration of SO_4^{2-} is identical to its value in the volcanic hot spring (Yoshiike, 2003). The correlation between SO_4^{2-} and Ca^{2+} is positive with a coefficient of 0.98 (Table 3). The SIs of gypsum and anhydrite in most of the thermal water samples are negative or zero (Table 5), which indicates that most of the samples are undersaturated with respect to gypsum and anhydrite. This suggests that the SO_4^{2-} concentrations of these thermal water resources may be controlled by a steady state dissolution process (Grasby et al., 2000). Therefore, SO_4^{2-} and Ca^{2+} are derived from the dissolution of evaporates such as gypsum and anhydrite. The correlation between Na^+ and Cl^- is positive with a correlation coefficient of 0.87 (Table 3), which implies a provenance involving salt (NaCl) dissolution. The major reservoir consists of T_1j^2, T_1j^3, and T_1j^4 strata, and the secondary reservoir is composed of T_2l and T_1j^1 carbonate strata with a total thickness of 540 m, as mentioned above. The T_1j^2 and T_1j^4 strata in the Sichuan basin were deposited during the regressive period in which seawater was separated, condensed, and salinized to form a salty lagoon and Sabkha sedimentation. Therefore, two sedimentary sequences with periodic marine carbonate→sulfate→chloride (NaCl) formed (Guo et al., 1996), which explains the high correlations between SO_4^{2-} and Ca^{2+} and between Na^+ and Cl^- (Table 3).

In the thermal water samples, HCO_3^- is not a predominant anion (Fig. 2); its molarity is much lower than that of SO_4^{2-}. This phenomenon results from the production of Ca^{2+} during the dissolution of gypsum or/and anhydrite, which involves solubility reduction of $CaCO_3$ and $CaMg(CO_3)_2$ and precipitation (e.g., Plummer et al., 1990; Bischoff et al., 1994; Dobrzyński, 2007; Jin et al., 2010). This phenomenon is called the common ion effect, which makes the SIs of calcite and dolomite positive (Table 5). This fact can be verified by the correlation coefficients, which are −0.65 for SO_4^{2-} and HCO_3^- and −0.63 for Ca^{2+} and HCO_3^- (Table 3).

The concentration of Mg^{2+} in the thermal water samples is 3–4 times the value for some volcanic hot springs (Yoshiike, 2003) and 10 times the value for the shallow karst water in Chongqing (Yang et al., 2013). The correlation coefficient for Mg^{2+} and HCO_3^- is −0.37 (Table 3), which indicates that this high concentration of Mg^{2+} is not derived from the dissolution of dolomite. This can be verified using the scatter diagram of Mg^{2+} and HCO_3^- (Fig. 4). If the data points are located around the line representing a 1:4 ratio, this suggests that the Mg^{2+} is derived from congruent dissolution of dolomite (Wang et al., 2006). It can be seen that most data points except nos. 11 and 21, are far from the line (Fig. 4), which suggests that Mg^{2+} in the most thermal water is not the result of congruent dissolution of dolomite (Wang et al., 2006). The data points of nos.

Table 5
Calculated SI of each thermal water sample. –: no datum.

Sample ID no.	Anhydrite	Calcite	Chalcedony	Dolomite	Fluorite	Goethite	Gypsum	Halite	Hematite	Quartz	Siderite	Talc
1	−0.5	0.7	0	1.4	0	9.3	−0.4	−9.3	20.6	0.4	0	2.4
2	−0.1	1	0	1.6	0.2	9.2	0	−9.3	20.4	0.4	−1.1	4.1
3	0	0.8	−0.1	1.3	0.1	8.1	0	−8.4	18.4	0.3	−1.9	3.5
4	−0.1	0.9	−0.1	1.4	0.2	9	0	−8.5	20.1	0.3	−1.2	3.8
5	−0.1	1.1	0	1.7	0.4	9	0	−9	20	0.4	−1.4	4.2
6	−0.1	1	0	1.7	0.2	9.1	0	−8.5	20.3	0.3	−1.4	4.7
7	−0.1	1	−0.1	1.7	0.2	9.1	0	−8.1	20.2	0.3	−1.5	4.8
8	−0.1	0.9	0	1.4	0.2	9	−0.1	−8.3	20.1	0.3	−1.3	4
9	−0.1	1	0	1.6	0.1	8.6	−0.1	−9.3	19.2	0.4	−1.8	4.6
10	−0.4	1	−0.1	1.7	0.2	8.2	−0.3	−8	18.4	0.3	−2.1	4.2
11	−2.1	1	0.4	1.9	−1.3	7.9	−1.9	−9.9	17.8	0.8	−2	5.1
12	−0.2	1.1	0.1	1.9	0.2	7.6	−0.1	−7.6	17.4	0.4	−2.9	5.4
13	−0.1	1.5	0	2.7	0.3	–	−0.1	−7.6	–	0.4	–	8.5
14	−0.3	1	−0.1	1.7	0	7.5	−0.3	−7.9	17.1	0.3	−2.6	3.8
15	−0.2	1.2	0	2.2	0.2	7.2	−0.2	−7.6	16.4	0.4	−3.5	6
16	−0.2	0.8	0.1	1.4	0.3	7.8	0	−7.3	17.7	0.5	−1.9	3.6
17	−0.2	0.7	0	1.1	0.3	7	−0.1	−7.4	16	0.4	−2.3	1.8
18	−0.2	1.6	0.2	2.9	0.4	8.5	0	−7.3	19	0.5	−3	8.7
19	−0.4	1	0	1.7	0.1	7.5	−0.2	−8.6	17.1	0.4	−2.4	3.4
20	−0.5	0.8	0	1.2	−0.4	8.3	−0.3	−9.4	18.7	0.4	−1.2	2
21	−1.7	−0.2	0	−1.2	−0.4	7.7	−1.5	−8.5	17.4	0.4	−1.1	−3
22	−0.1	1.1	−0.1	1.9	0.1	9.1	−0.1	−7.7	20.3	0.3	−1.6	5.4
23	−0.1	1.1	0	1.9	0.3	8.8	−0.1	−7.7	19.7	0.3	−1.9	5.2
24	−0.2	1	0.1	1.8	0.1	8.5	−0.1	−6.5	19.1	0.5	−2.1	5.7
25	−0.3	1	0.1	1.7	0.1	8.3	−0.2	−7.8	18.7	0.5	−1.8	4.5
26	−0.3	1.4	0	2.5	0.1	–	−0.2	−7.7	–	0.4	–	6.8
27	−0.3	1.3	0.2	2.3	0.1	8.4	−0.1	−8.4	19	0.5	−2.1	6.3
28	−0.2	1.2	0	2.1	0.1	8.4	−0.1	−8.4	18.9	0.3	−2	5
29	−0.1	1.1	0.1	1.6	0.5	7.8	0	−7.8	17.6	0.5	−2.4	3.8
30	−0.2	1	0.1	1.7	0.3	7.4	0	−7.8	17	0.5	−2.6	4.3
31	−0.1	1.1	0.1	2	0.2	8.2	0	−8.4	18.6	0.4	−2.4	6.1
32	0	1.2	0.1	2.1	0.1	7.6	0	−8.4	17.4	0.4	−3.2	6.5
33	0	1.3	0.1	2.1	0.2	7.9	0	−8.4	18	0.4	−3.1	6.5
34	−0.1	1	0.1	1.7	0.2	7.4	0	−8.4	17	0.5	−2.9	5
35	−0.1	0.9	0.1	1.4	0.2	8.3	0	−8.5	18.8	0.4	−1.8	4.2
36	−0.1	1.5	0.1	2.6	0.3	–	0	−8.3	–	0.5	–	8.3

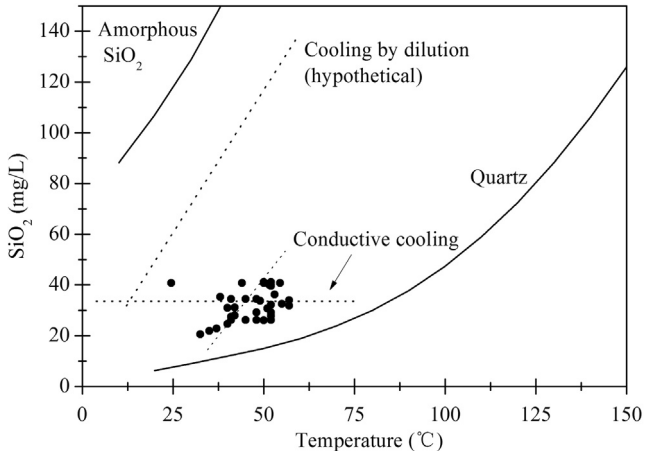

Fig. 3. Correlation between the SiO_2 concentration and the temperature reflecting the coupling of conductive cooling and dilution cooling.

11 and 21 are closer to the 1:4 line, which are attributed to the mixture of shallow karst groundwater. The correlation coefficient of 0.74 between Mg^{2+} and SO_4^{2-} demonstrates that the Mg^{2+} originates from the dissolution of magnesium sulfate.

In general, the concentrations of Ca^{2+} and SO_4^{2-} in the thermal water of the Chongqing main urban area are high due to the dissolution of gypsum or/and anhydrite, which can restrain the dissolution of carbonate and reduce the concentration of HCO_3^-.

5.2. Reservoir temperature and circulation depth

Care must be taken to select the appropriate geothermometer to estimate the reservoir temperature and avoid incorrect results or explanations. Distinct differences were observed among the reservoir temperatures (Table 4), which emphasizes the necessity of selecting a suitable geothermometer for the study area.

The Na-K-Mg Giggenbach diagram (Giggenbach, 1988) can be used to identify the water-rock equilibrium and the degree of mixing. As shown in Fig. 5, the data for all the thermal water samples are distributed in the right corner representing "immature water", which indicates possible mixing with cold water as the thermal water rises. Fig. 3 also demonstrates the potential effect of shallow cold water, which is to cause over- or under-estimated temperatures when cation thermometers, such as Na-K, Na-K-Ca, Na-Li, and K-Mg thermometers, are used (Table 4). Therefore, cation geothermometers are inappropriate for evaluating reservoir temperatures (Verma and Santoyo, 1997).

Some of the calculated temperatures given by the chalcedony thermometer (Fournier, 1977) listed in Table 4 are lower than the measured temperatures listed in Table 1. The average calculated temperature based on the chalcedony thermometer is 50.6 °C, which is slightly higher than the measured temperature (46.5 °C). Therefore, the chalcedony thermometer is not suitable.

The original SiO_2 content is preserved without significant loss during the ascent of the thermal water. No secondary equilibrium occurs, and the SiO_2 content is close to the solubility curve of quartz (Fig. 3). The stable SiO_2 content may be the result of conductive cooling in the upper low-temperature strata and

Table 6
δD and $\delta^{18}O$ in typical thermal water samples. δD and $\delta^{18}O$ are in ‰; the recharge altitude is in m; and the annual average air temperature is in °C.

Sample ID no.	δD	$\delta^{18}O$	Recharge altitude	Annual average air temperature
2	−52	−7.6	838	13.3
4	−61	−9.2	1130	10.4
15	−50	−7.7	778	13.9
16	−60	−9.1	1103	10.6
26	−56	−8.7	960	10.4
32	−57	−8.4	1013	10.4
33	−58	−8.1	1020	10.4
Mean value	−56	−8.4	977	11.3

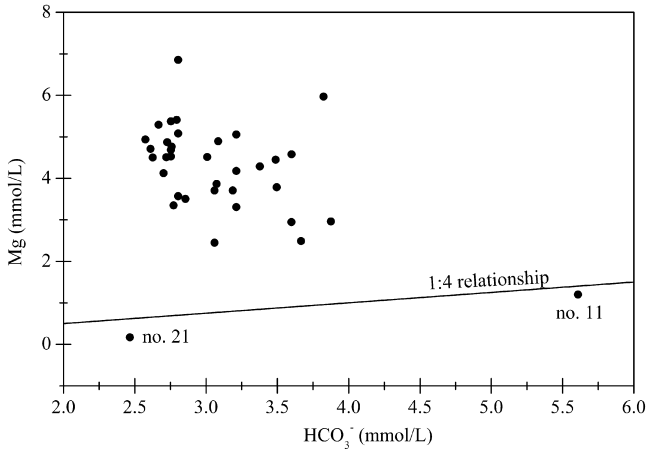

Fig. 4. Correlation between Mg^{2+} and HCO_3^- in the thermal water samples (modified from Wang et al., 2006). That most samples are far from the line representing a 1:4 ratio indicates that the dissolution of dolomite does not mainly contribute to the high concentration of Mg^{2+}.

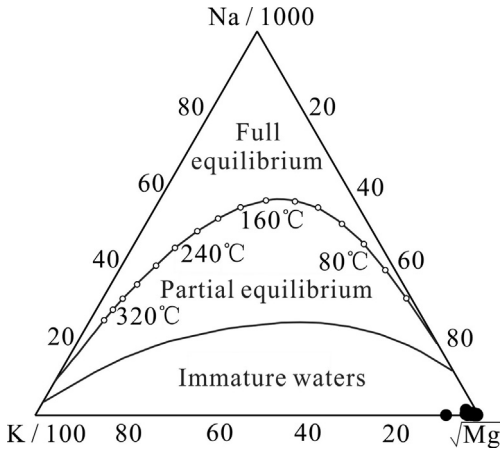

Fig. 5. Na–K–Mg Giggenbach plot (Giggenbach, 1988) of the thermal water samples. The water samples are located in the "immature water" region, which indicates that the thermal water mixes with the surface cold water.

diluted cooling by the cold surface water. Therefore, it is theoretically reliable to estimate the reservoir temperature using quartz and improved SiO_2 thermometers (Fournier, 1977; Verma and Santoyo, 1997), which yield reservoir temperatures of 64.6–93 °C and 65.1–93.7 °C, respectively, with average values of 81.8 °C and 82.5 °C, respectively. The average reservoir temperatures calculated using these two methods are between 64.8 and 93.4 °C (Table 4). When the reservoir's temperature is over 70 °C, the system achieves quartz equilibrium (Fournier, 1983). All the thermal water resources are oversaturated with quartz (Table 5 and Fig. 3). Additionally, most reservoir temperatures estimated using quartz geothermometers are higher than 70 °C (Fournier, 1983), which suggests that the quartz geothermometer is the best for this region.

The circulation depth is one of the significant factors influencing the reservoir's temperature, as well as one of the important parameters in geothermal studies that analyze the origin and formation mechanism of thermal water and assess potential geothermal reservoirs. The circulation depth calculated using Eq. (1) is 1579–2520 m with an average of 2150 m (Table 4), which is consistent with the reservoir depth revealed by the well. For example, in the well called Tong-5, which was drilled four km southeast of well no. 14 in 1993, the layer with low permeability at the bottom of the geothermal reservoir (T_1j) was 2002 m deep, which is approximately consistent with the estimated average circulation depth of 2150 m.

5.3. Recharge of the thermal water resources based on an isotopic analysis

The source of the water is an important factor when considering the heat source of thermal water. Hydrogen and oxygen isotopes can, to some extent, trace the circulation of water through the atmosphere and are, therefore, widely applied in studies of the origin of thermal water (e.g., Pastorelli et al., 1999; Chandrajith et al., 2013; Chatterjee et al., 2016). The values of δD and $\delta^{18}O$ obtained from seven wells, nos. 2, 4, 15, 16, 26, 32, and 33 (Table 6), are graphed and compared with the global meteoric water line (GMWL; Craig, 1961) and the Chongqing meteoric water line (CMWL; Li et al., 2010). As shown in Fig. 6, all the data points are close to the GMWL and the CMWL without shifting. This implies that local precipitation is the major factor in recharging the geothermal water, which is consistent with other studies demonstrating meteoric origins for thermal water around the world (e.g., Grasby et al., 2000; Ahmad et al., 2001; Lee et al., 2011; Moreira and Fernández, 2015), especially in carbonate reservoirs (e.g., Goldscheider et al., 2010; Sun et al., 2016).

The values of δD for the thermal water resources show that the recharge altitude can be calculated to be 838–1130 m using Eq. (2), with an average of 977 m (Table 6). The annual temperature of the recharge area ranges from 10.4 to 13.9 °C, according to Eq. (3), and the average is 11.3 °C (Table 6).

Dating by means of the radioactive carbon isotope ^{14}C is one of the most useful methods for dating groundwater that is between 1000 and 45,000 yrs old (Zhu and Murphy, 2000). This method has recently been well developed (Samborska et al., 2013). The ^{14}C data in this paper are from a geological investigation report (Chongqing Monitoring Station of Geological Environments, 2009). According to the ^{14}C analyses of nos. 2, 3, 5, and 8 at the Guanyinxia anticline, the ^{14}C ages increase from the north to the south from 14830 ± 220 to 17550 ± 250 yrs, which indicates that

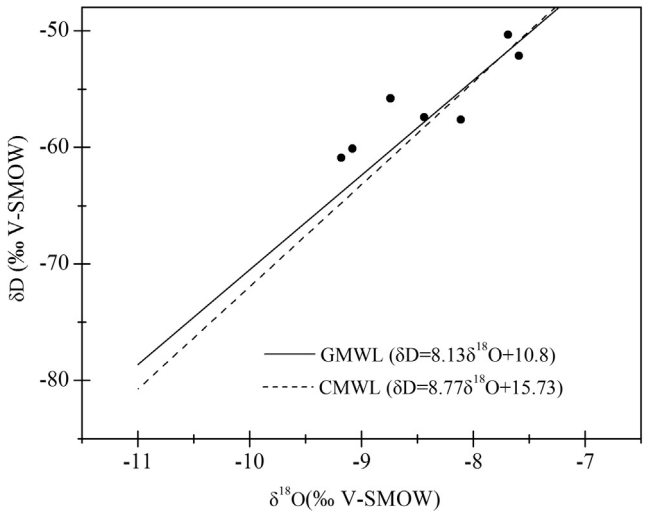

Fig. 6. Values of δD and $\delta^{18}O$ for the thermal water samples over the Global Meteoric Water Line (GMWL; Craig, 1961) and the Chongqing Meteoric Water Line (CMWL; Li et al., 2010).

the thermal water at the Guanyinxia anticline moves from the north to the south.

5.4. Conceptual model of thermal water circulation

In the surrounding area, Tongluoshan and Huayingshan, which are approximately 175 km northeast (Fig. 1a), satisfy the elevation (838–1130 m) and annual air temperature (11.3 °C) criteria for the thermal water recharge area. The elevation of the highest peak in these areas is 1704.1 m; the annual average temperature is 11.5 °C, and the average precipitation is 1282.2 mm (Luo et al., 2013).

On the basis of the above interpretation and discussion, a conceptual regional flow model shown in Fig. 7 is proposed; this model is not intended to represent the detailed heterogeneity and anisotropy of the system, rather only its main features. The presence of a structurally weak zone, such as a permeable fault, is more favorable for the percolation of meteoric water to shallow depths (Chandrajith et al., 2013). These regions exhibit two faults, the Tongluoshan fault and Huayingshan fault whose structure extends from northeast to southwest (Zhang et al., 2015; Shi et al., 2016) shown in Fig. 1a. Carbonate is widely distributed in the Tongluoshan and Huayingshan areas, especially on the exposed anticline; caves, sinkholes, shafts, and fractures are well developed and acts as unconfined carbonate outcrops and provide ideal channels for the vertical infiltration and recharge of meteoric water.

On the regional scale, groundwater movement from recharge to discharge areas is generally gravity (topography) driven (Tóth 1963; Jiang et al., 2012; Mádl-Szőnyi and Tóth, 2015; Mádl-Szőnyi and Simon, 2016). Meteoric water falling in the Tongluoshan and Huayingshan areas percolates to the geothermal reservoir and is heated continuously by the bedrock until it becomes thermal water. An ideal reservoir has a high hydraulic conductivity and large specific storage for long term productivity and is characterized by hydrostatic pressure-like conditions (Mádl-Szőnyi and Simon, 2016). Deep carbonate rocks are often more permeable than other reservoirs (Goldscheider et al., 2010). Based on information on the drilled wells in Chongqing, the geothermal reservoirs of the study area exhibit porosities of 3–4% (Cheng et al., 2015), which could provide good conditions to produce a high productivity rate of thermal water. The high topographic gradient between the higher altitude recharge areas of Tongluoshan, Huayingshan and the low-lying discharge zone in the main urban area of Chongqing drives the thermal water along the fault and the anticline core of the east Sichuan fold belts to the southwest (Figs. 1 and 7). The pattern of thermal groundwater flow in our study area characterized by confined carbonate is similar to the confined part of Budapest in Hungary, where intense heat accumulation could be established under the confined part of a carbonate basin (Mádl-Szőnyi and Tóth, 2015).

The residence time of the regional groundwater flow is relatively long; therefore, the water-rock interaction is sufficient to continuously dissolve evaporates during its transport (Fig. 7), which results in elevated TDS (Table 1). The dissolution of gypsum could increase the porosity and the permeability in the carbonate aquifer, which can provide an initial secondary porosity to allow the deep penetration of groundwater that is not saturated with calcite, and accelerate karstification and increase the productivity (Gunn et al., 2006). During the transport of the thermal water, the cover pressure is reduced along river cutting and in lower-elevation areas, which leads to natural exposures of thermal water

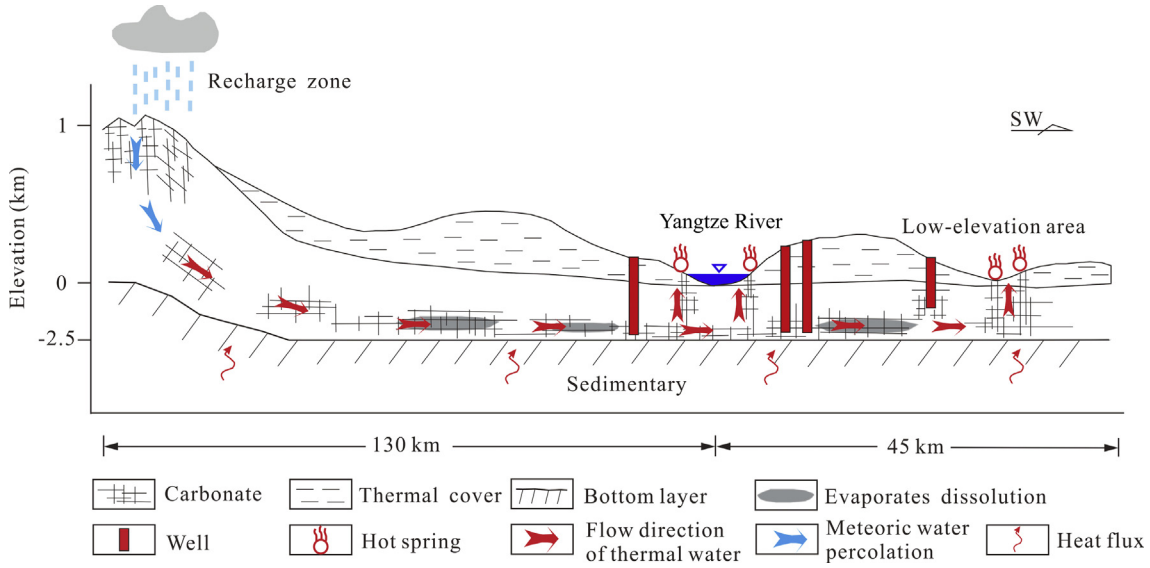

Fig. 7. Conceptual regional flow model of the circulation of thermal water. The horizontal and vertical scales in the model are not equal; some are decreased for visibility.

in the form of artesian hot springs that form a geothermal artesian karstic system, as in the case reported by Frumkin and Gvirtzman (2006) or drainage in the form of drilled wells.

6. Conclusion

The thermal water in the main urban area of Chongqing comes from the karst aquifer formed by Lower and Middle Triassic carbonate rock. Using its physical and chemical properties and the values of $\delta^{18}O$, δD, and $\delta^{14}C$, its origin, reservoir temperature, circulation depth, recharge, and drainage have been investigated.

The chemical types of most of the thermal water samples are Ca·Mg-SO_4 and Ca-SO_4. The independent sample *t*-test demonstrates that the well depth has no effect on the physical and chemical properties. Concentrated SO_4^{2-} and Ca^{2+} are formed through the dissolution of gypsum and anhydrite in the karst strata; the dissolution of carbonate is restrained by the common ion effect, which results in dilute HCO_3^-. Furthermore, Na^+ and Cl^- originate from the dissolution of salt in the strata.

The Na-K-Mg diagram shows that the thermal water is immature, which indicates that cation thermometers (Fournier and Truesdell, 1973; Fouillac and Michard, 1981; Giggenbach, 1988) cannot be used. Quartz (Fournier, 1977) and improved SiO_2 thermometers (Verma and Santoyo, 1997) are selected; they yield reservoir temperatures in the range from 64.8 to 93.4 °C and circulation depths from 1579 to 2520 m with an average of 2150 m.

The $\delta^{18}O$ and δD values for the thermal water samples are mainly distributed near the local meteoric water line. Combined with the region's geology and tectonic characteristics, a large volume of meteoric water infiltrates through the unconfined carbonate outcrops in the Tongluoshan and Huayingshanregions northeast of the study area. The meteoric water infiltrates through exposed carbonate karst channels to the geothermal reservoir. In this process, the water is continuously heated and driven by gravity along the fault and the anticline core to the southwest. In river cutting and lower-elevation areas, the water is exposed in artesian springs or drained in wells.

Acknowledgments

Special thanks are due to Wenjian Wu and Qiong Xiao, who generously provided the digital elevation model (DEM) data of the study area and one isotopic datum (sample no. 2), respectively. The authors also appreciate the constructive comments and suggestions by anonymous reviewers. Additional thanks are given to Xinyi Xiang for her valuable comments. This work was supported by the National Key Technology R&D Program of China (Grant Nos. 2011BAC09B01, 2016YFC050230206), the 2014 Scientific and Technical Program of the Land Resource and Housing Management Bureau of Chongqing, China (Grant No. CQGT-KJ-2014056), and the Fundamental Research Funds for Central Universities (Grant Nos. XDJK2014A016, XDJK2016E022, XDJK2016E023, XDJK2016E042, and XDJK2016D046).

References

Ahmad, M., Akram, W., Hussain, S.D., Sajjad, M.I., Zafar, M.S., 2001. Origin and subsurface history of geothermal water of Murtazabad area, Pakistan - an isotopic evidence. Appl. Radiat. Isot. 55 (5), 731–736. http://dx.doi.org/10.1016/S0969-8043(01)00119-1.

Bai, Y.T., Xu, Z.G., Zhang, J., Mao, D.Q., Luo, C., He, Y.Y., Liang, G.D., Lu, B., Bisesi, M.S., Sun, Q.H., Xu, X.Y., Yang, W.Z., Liu, Q.Y., 2014. Regional impact of climate on Japanese encephalitis in areas located near the Three Gorges Dam. PLoS ONE 9 (1), e84326. http://dx.doi.org/10.1371/journal.pone.0084326.

Bischoff, J.L., Juliá, R., Shanks III, W.C., Rosenbauer, R.J., 1994. Karstification without carbonic-acid: bedrock dissolution by gypsum-driven dedolomitization. Geol. 22 (11), 995–998. http://dx.doi.org/10.1130/0091-7613(1994) 022.

Can, I., 2002. A new improved Na/K geothermometer by artificial neural networks. Geothermics 31, 751–760. http://dx.doi.org/10.1016/S0375-6505(02)00044-5.

Chandrajith, R., Barth, J.A.C., Subasinghe, N.D., Merten, D., Dissanayake, C.B., 2013. Geochemical and isotope characterization of geothermal spring waters in Sri Lanka: evidence for steeper than expected geothermal gradients. J. Hydrol. 476, 360–369. http://dx.doi.org/10.1016/j.jhydrol.2012.11.004.

Chatterjee, S., Sharma, S., Ansari, M.A., Deodhar, A.S., Low, U., Sinha, U.K., Dash, A., 2016. Characterization of subsurface processes estimation of reservoir temperature in Tural Rajwadi geothermal fields, Maharashtra, India. Geothermics 59, 77–89. http://dx.doi.org/10.1016/j.geothermics.2015.10.011.

Cheng, Q., Yang, H., Zeng, M., 2015. The formation and protection of karst geothermal water resources in the main urban area of Chongqing. Carsologica Sin. 34 (3), 217–227. http://dx.doi.org/10.11932/karst20150303 (in Chinese with English abstract).

Chongqing Monitoring Station of Geological Environments, 2009. Survey and Effect Assessment of the Water Quality of Thermal Waters and Mineral Waters in the Main Urban Area of Chongqing (in Chinese).

Craig, H., 1961. Isotopic variations in meteoric waters. Science 133 (3465), 1702–1703. http://dx.doi.org/10.1126/science.133.3465.1702.

D'Amore, F., Ramos-Candelaria, M.N., Seastres Jr, J., Ruaya, J.R., Nuti, S., 1993. Applications of gas chemistry in evaluating physical processes in the southern Negros (Palinpinon) geothermal field, Philippines. Geothermics 22, 535–553. http://dx.doi.org/10.1016/0375-6505(93)90035-L.

Dobrzyński, D., 2007. Chemical diversity of groundwater in the Carboniferous-Permian aquifer in the Unisław Śląski - Sokołowsko area (the Sudetes, Poland); a geochemical modelling approach. Acta Geol. Pol. 57 (1), 97–112.

Domenico, P.A., Palciauskas, V.V., 1973. Theoretical analysis of forced convective heat-transfer in regional groundwater flow. Geol. Soc. Am. Bull. 84 (12), 3803–3814. http://dx.doi.org/10.1130/0016-7606(1973) 84<3803:Taofch>2.0.Co;2.

Fouillac, C., Michard, G., 1981. Sodium/lithium ratio in water applied to geothermometry of geothermal reservoirs. Geothermics 10, 55–70. http://dx.doi.org/10.1016/0375-6505(81)90025-0.

Fournier, R.O., 1977. Chemical geothermometers and mixing models for geothermal systems. Geothermics 5, 41–50. http://dx.doi.org/10.1016/0375-6505(77)90007-4.

Fournier, R.O., 1983. A method of calculating quartz solubilities in aqueous sodium chloride solutions. Geochim. Cosmochim. Acta 47 (1–4), 579–586. http://dx.doi.org/10.1016/0016-7037(83)90279-X.

Fournier, R.O., Truesdell, A.H., 1973. An empirical Na-K-Ca geothermometer for natural waters. Geochim. Cosmochim. Acta 37 (3), 1255–1275. http://dx.doi.org/10.1016/0016-7037(73)90060-4.

Frumkin, A., Gvirtzman, H., 2006. Cross-formational rising groundwater at an artesian karstic basin: the Ayalon Saline Anomaly. Israel. J. Hydrol. 318 (1–4), 316–333. http://dx.doi.org/10.1016/j.jhydrol.2005.06.026.

Giggenbach, W.F., 1988. Geothermal solute equilibria. Derivation of Na-K-Mg-Ca geoindicators. Geochim. Cosmochim. Acta 52, 2749–2765. http://dx.doi.org/10.1016/0016-7037(88)90143-3.

Goldscheider, N., Mádl-Szőnyi, J., Erőss, A., Schill, E., 2010. Review: thermal water resources in carbonate rock aquifers. Hydrogeol. J. 18 (6), 1303–1318. http://dx.doi.org/10.1007/s10040-010-0611-3.

Grasby, S.E., Hutcheon, I., Krouse, H.R., 2000. The influence of water-rock interaction on the chemistry of thermal springs in western Canada. Appl. Geochem. 15 (4), 439–454. http://dx.doi.org/10.1016/S0883-2927(99)00066-9.

Gunn, J., Bottrell, S.H., Lowe, D.J., Worthington, S.R.H., 2006. Deep groundwater flow and geochemical processes in limestone aquifers: evidence from thermal waters in Derbyshire, England, UK. Hydrogeol. J. 14 (6), 868–881. http://dx.doi.org/10.1007/s10040-006-0022-7.

Guo, Z., Deng, K., Han, Y., Liu, Y., 1996. The Formation and Development of Sichuan Basin. Geological Press, Beijing (in Chinese).

Jiang, X.W., Wan, L., Ge, S., Cao, G.L., Hou, G.C., Hu, F.S., Wang, X.S., Li, H.L., Liang, S. H., 2012. A quantitative study on accumulation of age mass around stagnation points in nested flow systems. Water Resour. Res. 48 (12), 771–784. http://dx.doi.org/10.1029/2012WR012509.

Jiang, X.W., Wang, X.S., Wan, L., Ge, S., 2011. An analytical study on stagnant points in nested flow systems in basins with depth-decaying hydraulic conductivity. Water Resour. Res. 47 (1), 128–139. http://dx.doi.org/10.1029/2010WR009346.

Jin, L., Siegel, D.I., Lautz, L.K., Mitchell, M.J., Dahms, D.E., Mayer, B., 2010. Calcite precipitation driven by the common ion effect during groundwater–surface-water mixing: a potentially common process in streams with geologic settings containing gypsum. Geol. Soc. Am. Bull. 122 (7–8), 1027–1038. http://dx.doi.org/10.1130/B30011.1.

Kong, Y., Pang, Z., Shao, H., Hu, S., Kolditz, O., 2014. Recent studies on hydrothermal systems in China: a review. Geotherm. Energy 2, 19. http://dx.doi.org/10.1186/s40517-014-0019-8.

Lee, S., Kim, T., Lee, T.J., 2011. Strontium isotope geochemistry and its geochemical implication from hot spring waters in South Korea. J. Volcanol. Geotherm. Res. 208 (1–2), 12–22. http://dx.doi.org/10.1016/j.jvolgeores.2011.09.004.

Li, D., Liu, D., 2011. Geothermal reservoir structure and runoff flow recharge of geothermal water resources in Chongqing City. J. Hohai Univ. (Nat. Sci.) 39(4), 372–376. http://dx.doi.org/10.3876/j.issn.1000-1980.2011.04.004 (in Chinese with English abstract).

Li, T., Li, H., Shen, C., Yang, C., Li, J., Yi, C., Yuan, D., Wang, J., Xie, S., 2010. Study on the δD and δ18O characteristics of meteoric precipitation during 2006–2008 in Chongqing. Adv. Water Sci. 21 (6), 757–764 (in Chinese with English abstract).

Lund, J.W., Freeston, D.H., Boyd, T.L., 2011. Direct utilization of geothermal energy 2010 worldwide review. Geothermics 40, 159–180. http://dx.doi.org/10.1016/j.geothermics.2011.07.004.

Luo, P., Qin, Z., Sun, C., 2013. The geological heritage resources system of Huayingshan Grand Canyon Geo-park in Sichuan and its geographic significance. Acta Geosci. Sinica 34 (6), 738–748. http://dx.doi.org/10.3975/cagsb.2013.06.11 (in Chinese with English abstract).

Mádl-Szőnyi, J., Simon, S., 2016. Involvement of preliminary regional fluid pressure evaluation into the reconnaissance geothermal-exploration-Example of an overpressured and gravity-driven basin. Geothermics 60, 156–174. http://dx.doi.org/10.1016/j.geothermics.2015.11.001.

Mádl-Szőnyi, J., Tóth, A., 2015. Basin-scale conceptual groundwater flow model for an unconfined and confined thick carbonate region. Hydrogeol. J. 23 (7), 1359–1380. http://dx.doi.org/10.1007/s10040-015-1274-x.

Majumdar, N., Mukherjee, A.L., Majumdar, R.K., 2009. Mixing hydrology and chemical equilibria in Bakreswar geothermal area, Eastern India. J. Volcanol. Geotherm. Res. 183 (3–4), 201–212. http://dx.doi.org/10.1016/j.jvolgeores.2009.03.014.

Millot, R., Négrel, P., 2007. Multi-isotopic tracing (δ^7Li, δ^{11}B, ^{87}Sr/^{86}Sr) and chemical geothermometry: evidence from hydro-geothermal systems in France. Chem. Geol. 244 (3–4), 664–678. http://dx.doi.org/10.1016/j.chemgeo.2007.07.015.

Moreira, P., Fernández, R.R., 2015. La Josefina Au-Ag deposit (Patagonia, Argentina): a Jurassic epithermal deposit formed in a hot spring environment. Ore Geol. Rev. 67, 297–313. http://dx.doi.org/10.1016/j.oregeorev.2014.12.012.

Parkhurst, D.L., Appelo, C.A.J., 2013. Description of input and examples for PHREEQC version 3 – A computer program for speciation, batch-reaction, one-dimensional transport, and inverse geochemical calculations. Chapter 43 of Section A, Groundwater Book 6, Modeling Techniques, <http://pubs.usgs.gov/tm/06/a43/>.

Pastorelli, S., Marini, L., Hunziker, J.C., 1999. Water chemistry and isotope composition of the Acquarossa thermal system, Ticino, Switzerland. Geothermics 28, 75–93. http://dx.doi.org/10.1016/S0375-6505(98)00045-5.

Pérez-Zárate, D., Santoyo, E., Guevara, M., Torres-Alvarado, I.S., Peiffer, L., Martínez-Frías, J., 2015. Geochemometric modeling and geothermal experiments of water/rock interaction for the study of alkali-feldspars dissolution. Appl. Therm. Eng. 75, 1244–1261. http://dx.doi.org/10.1016/j.applthermaleng.2014.09.011.

Plummer, L.N., Busby, J.F., Lee, R.W., Hanshaw, B.B., 1990. Geochemical modeling of the Madison aquifer in parts of Montana, Wyoming, and South-Dakota. Water Resour. Res 26 (9), 1981–2014. http://dx.doi.org/10.1029/Wr026i009p01981.

Samborska, K., Różkowski, A., Małoszewski, P., 2013. Estimation of groundwater residence time using environmental radioisotopes (^{14}C, T) in carbonate aquifers, southern Poland. Isot. Environ. Healt. Stud. 49 (1), 73–97. http://dx.doi.org/10.1080/10256016.2012.677041.

Schipper, L.A., McGill, A., 2008. Nitrogen transformation in a denitrification layer irrigated with dairy factory effluent. Water Res. 42 (10–11), 2457–2464. http://dx.doi.org/10.1016/j.watres.2008.01.033.

Shi, H., Shi, X., Glasmacher, U.A., Yang, X., Stockli, D.F., 2016. The evolution of eastern Sichuan basin, Yangtze block since Cretaceous: constraints from low temperature thermochronology. J. Asian Earth Sci. 116, 208–221. http://dx.doi.org/10.1016/j.jseaes.2015.11.008.

Sun, Z.Y., Ma, R., Wang, Y.X., Ma, T., Liu, Y.D., 2016. Using isotopic, hydrogeochemical-tracer and temperature data to characterize recharge and flow paths in a complex karst groundwater flow system in northern China. Hydrogeol. J 24 (6), 1393–1412. http://dx.doi.org/10.1007/s10040-016-1390-2.

The Geological and Mineral of the People's Republic of China, 1993. Detection Method of Groundwater (DZ/T 0064.1∼0063.80-93) (in Chinese).

Tóth, J., 1962. A theory of groundwater motion in small drainage basins in central Alberta, Canada. J. Geophys. Res. 67 (11), 4375–4388. http://dx.doi.org/10.1029/Jz067i011p04375.

Tóth, J., 1963. A theoretical analysis of groundwater flow in small drainage basins. J. Geophys. Res. 68 (16), 4795–4812. http://dx.doi.org/10.1029/Jz068i008p02354.

Tóth, J., 1995. Hydraulic continuity in large sedimentary basins. Hydrogeol. J. 3 (4), 4–16. http://dx.doi.org/10.1007/s100400050250.

Tóth, J., 2009. Gravitational systems of groundwater flow. In: Theory, Evaluation, Utilization. Cambridge University Press, Cambridge.

Verma, S.P., Santoyo, E., 1997. New improved equations for Na/K, Na/Li and SiO_2, geothermometers by outlier detection and rejection. J. Volcanol. Geotherm. Res. 79, 9–23. http://dx.doi.org/10.1016/S0377-0273(97)00024-3.

Wang, G., Li, K., Wen, D., Lin, W., Lin, L., Liu, Z., Zhang, W., Ma, F., Wang, W., 2015. Assessment of geothermal resources in China. In: Proceedings of the World Geothermal Congress 2015, Melbourne, Australia.

Wang, S., Pang, Z., Liu, J., Lin, P., Liu, S., Yin, M., 2013. Origin and evolution characteristics of geothermal water in the Niutuozhen geothermal field, North China Plain. J. Earth Sci. 24 (6), 891–902. http://dx.doi.org/10.1007/s12583-013-0390-6.

Wang, Y., Guo, Q., Su, C., Ma, T., 2006. Strontium isotope characterization and major ion geochemistry of karst water flow, Shentou, northern China. J. Hydrol. 328 (3–4), 592–603. http://dx.doi.org/10.1016/j.jhydrol.2006.01.006.

Xiao, Q., Shen, L., Yang, L., 2015. Analysis on origin and recharge mechanism of geothermal water, a case study of Beiwenquan hot spring in Chongqing, China. J. Chongqing Univ. 38 (4), 91–103. http://dx.doi.org/10.11835/j.issn.1000-582X.2015.04014 (in Chinese with English abstract).

Yang, P., Yuan, D., Ye, X., Xie, S., Chen, X., Liu, Z., 2013. Sources and migration path of chemical compositions in a karst groundwater system during rainfall events. Chin. Sci. Bull. 58 (20), 2488–2496. http://dx.doi.org/10.1007/s11434-013-5762-x.

Yoshiike, Y., 2003. Variation in the chemical composition of Obuki Spring, Tamagawa Hot Springs (1951–2000). Geochem. J. 37 (6), 649–662.

Zhang, X., Zha, X., Dai, Z., 2015. Stress changes induced by the 2008 Mw7:9 Wenchuan earthquake, China. J. Asian Earth Sci. 98, 98–104. http://dx.doi.org/10.1016/j.jseaes.2014.10.001.

Zhao, X., Wan, G., 2014. Current situation and prospect of China's geothermal resources. Renew. Sustain. Energy Rev. 32, 651–661. http://dx.doi.org/10.1016/j.rser.2014.01.057.

Zhou, X., Jin, X., Liang, S., Shen, Y., Zhang, H., 2010. Monograph of Groundwater Sciences. Geological Press, Beijing (in Chinese).

Zhu, C., Murphy, W.M., 2000. On radiocarbon dating of ground water. Ground Water 38 (6), 802–804. http://dx.doi.org/10.1111/j.1745-6584.2000.tb00671.x.

Zijl, W., 1999. Scale aspects of groundwater flow and transport systems. Hydrogeol. J. 7 (1), 139–150. http://dx.doi.org/10.1007/s100400050185.